Rapid Communications

Plasmonic Landau damping in active environments

Niket Thakkar,[1,*] Nicholas P. Montoni,[2] Charles Cherqui,[2] and David J. Masiello[1,2,†]
[1]*Department of Applied Mathematics, University of Washington, Seattle, Washington 98195-3925, USA*
[2]*Department of Chemistry, University of Washington, Seattle, Washington 98195-1700, USA*

(Received 18 April 2017; revised manuscript received 31 January 2018; published 12 March 2018)

Optical manipulation of charge on the nanoscale is of fundamental importance to an array of proposed technologies from selective photocatalysis to nanophotonics. Open plasmonic systems where collective electron oscillations release energy and charge to their environments offer a potential means to this end as plasmons can rapidly decay into energetic electron-hole pairs; however, isolating this decay from other plasmon-environment interactions remains a challenge. Here we present an analytic theory of noble-metal nanoparticles that quantitatively models plasmon decay into electron-hole pairs, demonstrates that this decay depends significantly on the nanoparticle's dielectric environment, and disentangles this effect from competing decay pathways. Using our approach to incorporate embedding material and substrate effects on plasmon-electron interaction, we show that predictions from the model agree with four separate experiments. Finally, examination of coupled nanoparticle-emitter systems further shows that the hybridized in-phase mode more efficiently decays to photons whereas the out-of-phase mode more efficiently decays to electron-hole pairs, offering a strategy to tailor open plasmonic systems for charge manipulation.

DOI: 10.1103/PhysRevB.97.121403

Localized surface-plasmon (LSP) resonances, the collective oscillations of conduction-band electrons in noble-metal nanoparticles (MNPs), have a fundamental role in nanoscale optics and electronics [1]. These collective phenomena offer unique control of light [1,2], heat [3,4], and charge [5,6] in nanoscale systems, and studies of their basic properties continue to promise new applications in a range of fields from selective catalysis [7] to quantum computing [8]. The interconversion of LSPs to individual electronic excitations, so-called Landau damping [9], has gained particular experimental interest [5,10–13]. Studies report changes in LSP spectra due to changes in particle environment, such as substrate or embedding material [11–13], as potential signatures of enhanced interconversion rates, indicating that Landau damping depends on the MNP's dielectric environment in analogy to Purcell enhancement of a fluorescent molecule's radiative decay [14]. Still, disentangling Landau damping from other effects, such as optical energy transfer [15], presents significant experimental challenges and complicates the interpretation of results. A theory of LSP-electron interaction capable of incorporating environmental effects from substrates to other optical emitters is needed to guide experiments and offer a platform to optimize nanoparticle systems for electron-hole pair generation.

Landau damping is known to increase with decreasing MNP size [16–18] and is most significant at length scales where classical descriptions of LSPs require quantum-mechanical modification. Recent research on MNPs [19–22], MNP aggregates [23], and bulk metals [24–27] has confirmed this result while emphasizing the importance of an accurate description of the metal's electronic structure, electron spill out, and nonlocal dielectric effects. Meanwhile, a large body of research has taken quantum descriptions of small metal clusters and has worked to develop atomistic models of LSPs in larger clusters [28–35]. In most cases, however, MNPs are described in isolation, and the incorporation of environmental effects is often computationally intractable.

In this Rapid Communication, we present a quantitatively accurate analytic theory of Landau damping in noble metals, accounting for optically active environments. We compare the theory to four experiments: the photofragmentation spectroscopy by Tiggesbäumker *et al.* [36] on silver clusters in vacuum, the matrix deposition spectroscopies by Charlé *et al.* [37] and Harbich *et al.* [38] on silver clusters in argon, and the electron energy-loss spectroscopy (EELS) by Scholl *et al.* [39] on silver nanospheres on 3-nm carbon substrates. After incorporating dielectric background and substrate effects, we demonstrate that the theory reproduces the observed LSP energies in all four experiments over decades of cluster sizes from $\sim$245 000 atoms to 5 atoms, reconciling experiments previously thought to disagree [28] and showing the environmental effects' role in determining quantum LSP properties. We conclude by generalizing the theory to predict the quantum-corrected energies of hybrid LSP-emitter systems relevant to studies of nanoparticle assemblies [40], MNP-quantum dot systems [41], and LSP-enhanced molecular spectroscopies [42]. Surprisingly, we find that, unlike the radiative properties of LSP-emitter systems [43], the hybridized out-of-phase LSP-emitter mode decays to electron-hole pairs most efficiently, and we suggest future experiments to measure this effect.

To elucidate the mechanism by which LSPs disintegrate into electron-hole pairs, we first consider an isolated silver nanosphere. The inset of Fig. 1(a) depicts a sphere with radius a characterized by infinite frequency dielectric response ε_1, modeling screening due to core electrons [16,18,39], and plasma

*thakkar@uw.edu
†masiello@chem.washington.edu

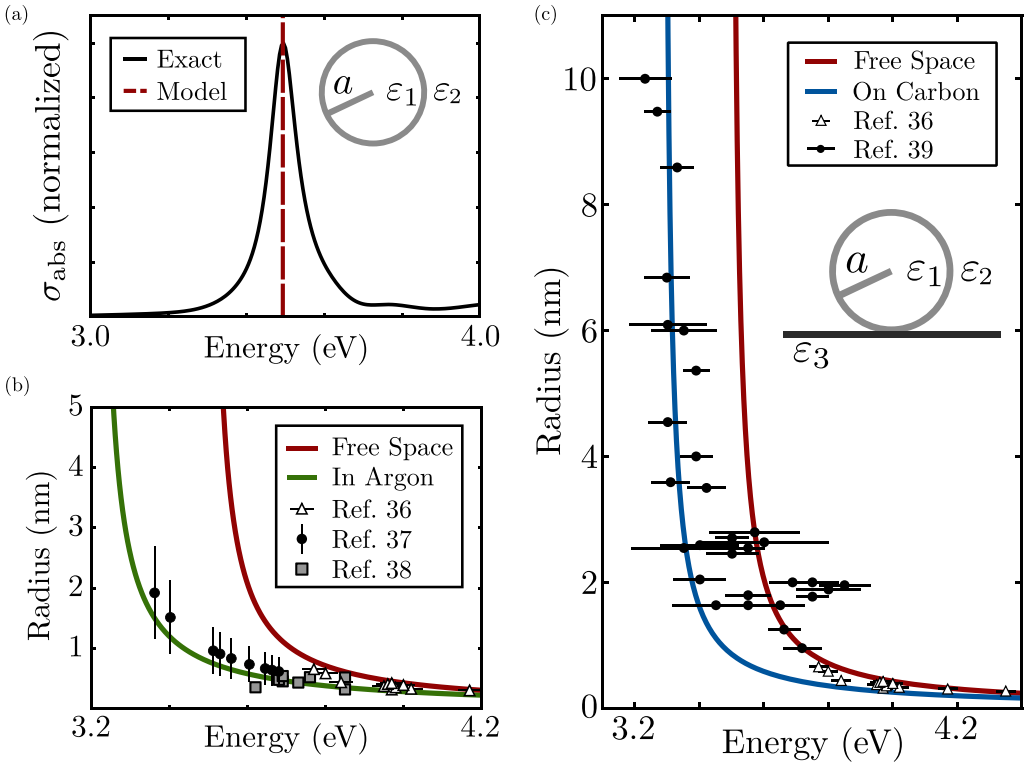

FIG. 1. Predictions and validations of the model. (a) The silver nanosphere's (the inset) absorption cross section is computed with Mie theory (the black curve) and compared to $\hbar\omega_{10}$ (the red dashed line) for $a = 10$ nm and $\varepsilon_2 = 1$, confirming the model's reproduction of classical results. (b) Comparison of the free space ($\varepsilon_2 = 1$, the red line) and argon-embedded ($\varepsilon_2 = 1.7$ [44], the green line) LSP energy to photofragmentation spectroscopy in vacuum (the white triangles, one standard deviation error bars) [36] and matrix deposition spectroscopies [37,38] in argon (the black circles with one standard deviation error bars and gray boxes). Quantitative agreement between the theory and the experiments shows that the theory effectively incorporates embedding dielectric effects. (c) Comparison of the LSP energy to EELS on a carbon substrate (the black circles, two standard deviation error bars) [39] with data from Ref. [36] for reference. When the model is extended to incorporate the carbon substrate (the blue curve, $\varepsilon_2 = 1$, $\varepsilon_3 = 3$), the predicted renormalized LSP energies agree excellently with measurement.

frequency ω_p embedded in material with dielectric constant ε_2. Both ε_1 and ω_p are estimated by fitting a frictionless free-electron (Drude) model to optical frequency dielectric data [45] for bulk silver (see the Supplemental Material (SI) [46]).

In the SI [46], we consider conduction electrons confined to the MNP by a potential $U_+(\mathbf{x})$ and show that their mean-field Coulomb interaction gives rise to a set of multipolar oscillators corresponding to particle-localized collective electronic motion, so-called LSPs [47]. The system's Hamiltonian is

$$H_{\text{free}} = \sum_i \left[\frac{\mathbf{p}_i^2}{2m_e} + U_+(\mathbf{x}_i)\right] + \sum_{\ell m}\left(\frac{V_{\ell m}}{2}|p_{\ell m}|^2 + \frac{\omega_{\ell m}^2}{2V_{\ell m}}|q_{\ell m}|^2\right) - \frac{e}{2m_e c}\sum_i [\mathbf{p}_i \cdot \mathbf{A}(\mathbf{x}_i) + \mathbf{A}(\mathbf{x}_i)\cdot \mathbf{p}_i], \tag{1}$$

where $q_{\ell m}$ and $p_{\ell m}$ are generalized LSP coordinates and momenta defined by the total conduction electron density's projection onto the ℓ,m multipole moments' field within the nanosphere. When retardation effects across the MNP are neglected [18], these projections oscillate with frequencies $\omega_{\ell m} = \sqrt{\ell\omega_p^2/[\ell\varepsilon_1 + (\ell+1)\varepsilon_2]}$ and mode volumes $V_{\ell m} = \{3/[\ell\varepsilon_1 + (\ell+1)\varepsilon_2]\}V_s$ where V_s is the sphere's volume. Equation (1) also introduces the electron positions $\mathbf{x}_i$ and momenta $\mathbf{p}_i$, which couple to the collective motion through $\mathbf{A}(\mathbf{x})$, the LSP vector potential. It is this interaction that governs Landau damping.

The validity of our estimates of ε_1 and ω_p can be assessed by comparing the model's prediction for the LSP energy [46] with that from Mie theory [48], the exact solution to Maxwell's equations for a dielectric sphere. This is performed in Fig. 1(a) where the model's predicted absorption resonance under z-polarized plane-wave excitation (the red dashed line) is compared to the Mie solution for an $a = 10$-nm silver nanosphere computed with complex-valued bulk dielectric data [45] (the black line). We see that the predicted resonance energy agrees with the exact solution and that the excitation source selects only the $\ell = 1$, $m = 0$ LSP mode, confirming that the MNP's optical properties are dipole dominated at small radii [16,18,39].

We now quantize H_{free} and calculate the leading-order effects of electron-plasmon interaction perturbatively. $U_+(\mathbf{x})$

is modeled as an infinite spherical well, and the resulting electron wave functions and energies are specified in Ref. [16]. Although this approximation neglects the complexity of silver's band structure and electron spill out at small sizes, an important effect in alkali metals [22], we show below that this greatly simplified electronic structure is sufficient for describing environmental effects on the noble MNPs of interest here.

To calculate the decay rate for LSPs to electron-hole pairs, we consider transitions between the initial and the final Fock states $|\varphi_i\rangle = |1_{10};0_e,0_h\rangle$ and $|\varphi_f\rangle = |0_{10};1_e,1_h\rangle$ of the form $|N_{\ell m};n_e,n_h\rangle$ with $N_{\ell m}$ plasmons in the ℓ,m mode, and n_e (n_h) electrons (holes) with quantum numbers e (h). All omitted occupation numbers are equal to zero, and the restriction to $\ell = 1$, $m = 0$ is based on the discussion of Fig. 1(a).

Using Fermi's golden rule with the interaction Hamiltonian in Eq. (1), we find the LSP decay rate to electron-hole pairs [46],

$$\Gamma_{\text{free}}(\omega_{10}, V_{10}) = \frac{64 V_{10}}{3\pi^3 V_s}\frac{e^2}{\hbar a}\int_{x_0}^{1}\frac{dx}{\nu^3}\sqrt{x^3(x+\nu)}, \qquad (2)$$

where $\nu = \hbar\omega_{10}/\epsilon_F$, $\epsilon_F = 5.5$ eV is the Fermi energy of silver [16] and $x_0 = \max\{0, 1-\nu\}$. Note $\Gamma_{\text{free}} \propto 1/a$, demonstrating that Landau damping becomes more significant as MNP size decreases, in qualitative agreement with previous studies [16–20]. Γ_{free} can also be used to approximate the second-order change in LSP energy, resulting in the renormalized energy $\hbar\omega_{10}^* \approx \sqrt{(\hbar\omega_{10} + \hbar\Gamma_{\text{free}})^2 - (\hbar\Gamma_{\text{free}}/2)^2}$.

In Fig. 1(b), we compare $\hbar\omega_{10}^*$ to photofragmentation spectroscopy [36] of silver clusters in free space ($\varepsilon_2 = 1$, the red line) and to matrix deposition spectroscopies [37,38] of silver clusters embedded in argon ($\varepsilon_2 = 1.7$ [44], the green line). We see that $\hbar\omega_{10}^*$ rapidly blueshifts as a decreases in excellent agreement with the datasets, validating our approximations and indicating that our theory effectively incorporates the embedding dielectric. Although not obvious, we show in the SI [46] that Γ_{free} increases with the embedding dielectric constant ε_2. Thus, LSP decay to electron-hole pairs is faster for MNPs in high dielectric materials since the plasmon field is more confined to the particle's interior and electron-plasmon interaction is therefore larger.

In Fig. 1(c), we further compare $\hbar\omega_{10}^*$ in free space (the red line) to data obtained via EELS on a 3-nm carbon substrate [39]. The prediction only qualitatively agrees with the blueshift in the EELS data, generally overestimating the measured LSP energy. Although it is possible to modify ε_1 and ω_p to shift our estimate to lower energies, this would be at the expense of agreement with Mie theory [Fig. 1(a)]. This check is critical since simultaneous agreement with Mie theory and measurement at small sizes shows that the model correctly transitions from quantum to classical electrodynamics. Thus, we instead extend the theory to include substrate effects, demonstrating that the resulting LSP energies agree with Mie theory and all four experiments [36–39] simultaneously.

The $\ell = 1$, $m = 0$ LSP field outside the MNP is identical to that of a point dipole located at the sphere's center [46]. This observation motivates using the method of images to incorporate the substrate. A point dipole with dipole moment $\mathbf{d}$ located above an infinite plane with dielectric constant ε_3 induces an image dipole $\mathbf{d}_I = -\mathbf{d}(\varepsilon_3 - \varepsilon_2)/(\varepsilon_3 + \varepsilon_2)$ in the opposite direction for the experimentally relevant case of $\varepsilon_3 > \varepsilon_2$ [15]. Although the substrates in experiments have finite thicknesses, the dominant image contribution is that of the infinite half-space [49], which we verify by accounting for the finite substrate in the SI [46]. Here, for simplicity, we model the substrate as infinite [Fig. 2(a), the inset], and we modify H_{free} to include $\mathbf{d}_I$,

$$H_{\text{sub}} = H_{\text{free}} - \mathbf{d}_{10}\cdot\mathbf{E}_I - \frac{e}{2m_e c}\sum_i[\mathbf{p}_i\cdot\mathbf{A}_I(\mathbf{x}_i) + \mathbf{A}_I(\mathbf{x}_i)\cdot\mathbf{p}_i], \qquad (3)$$

where $\mathbf{d}_{10}$ is the LSP dipole moment and $\mathbf{E}_I$ and $\mathbf{A}_I$ are the image electric field and vector potential. Here it is evident that the substrate affects the MNP, both through LSP coupling and through modification of the vector potential within the particle.

The LSP coupling can be diagonalized via transformation leading to a substrate-dressed LSP with mode volume $\tilde{V}_{10} = V_{10} - 2g$ and resonance frequency $\tilde{\omega}_{10} = \sqrt{\omega_{10}^2(1 - 2g/V_{10})}$

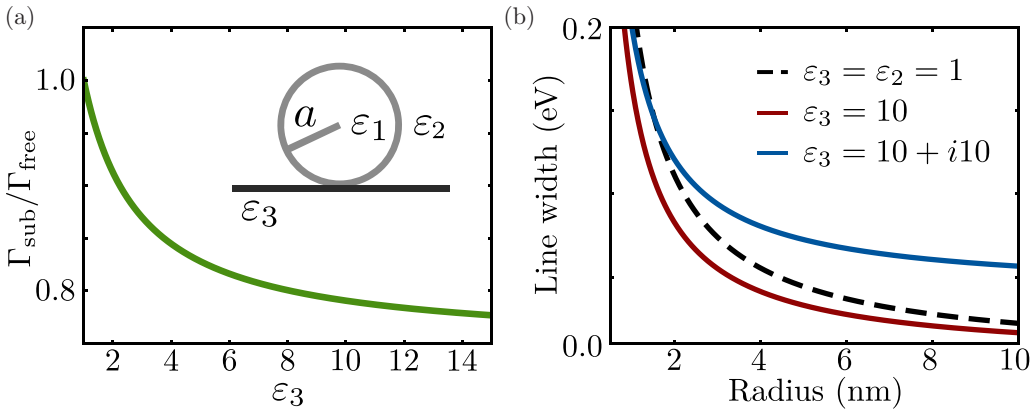

FIG. 2. (a) Substrate-dressed Landau damping relative to Γ_{free} as a function of ε_3. Suppression of the decay rate quickly saturates as ε_3 increases. Thus, the change in optical properties from free space ($\varepsilon_3 = 1$) to any substrate ($\varepsilon_3 > 1$) is large compared to the change between low and high dielectric substrates. (b) Size dependence of the substrate-modified LSP linewidth accounting for LSP-electron interaction and intrinsic substrate losses. The black dashed line shows Γ_{free}, and if ε_3 is complex valued (the blue curve), intrinsic substrate losses can cause an increase in linewidth, pushing the system into a regime where LSP decay to electron-hole pairs and to near-field interaction compete.

where $g = \pi a^3(\varepsilon_3 - \varepsilon_2)(\varepsilon_1 - \varepsilon_2)^2/6(\varepsilon_3 + \varepsilon_2)(\varepsilon_1 + 2\varepsilon_2)^2$, and we assume $\mathbf{d}_{10}$ is parallel to the substrate. This indicates in agreement with other studies [13] that the LSP mode volume and energy both decrease due to electrostatic substrate effects.

The remaining interaction term modifies the perturbation theory above. The LSP decay rate can be recalculated under the approximation that the image vector potential operator $\mathbf{A}_I(\mathbf{x}_i)$ can be treated as $\mathbf{A}_I(\langle \mathbf{x}_i \rangle)$. This approximation is valid since fluctuations of the electron position will destructively interfere as the number of electrons increases. The perturbation theory gives

$$\Gamma_{\text{sub}}(\tilde{\omega}_{10}, \tilde{V}_{10}) = |1-\alpha|^2 \frac{64\tilde{V}_{10}}{3\pi^3 V_s}\frac{e^2}{\hbar a}\int_{\tilde{x}_0}^{1}\frac{dx}{\tilde{\nu}^3}\sqrt{x^3(x+\tilde{\nu})}$$
$$= |1-\alpha|^2 \Gamma_{\text{free}}(\tilde{\omega}_{10}, \tilde{V}_{10}) \quad (4)$$

for the substrate-modified rate of LSP decay into electron-hole pairs. Here $\tilde{\nu} = \hbar\tilde{\omega}_{10}/\epsilon_F$, $\tilde{x}_0 = \max\{0, 1-\tilde{\nu}\}$, and $\alpha = (\varepsilon_1 - \varepsilon_2)(\varepsilon_3 - \varepsilon_2)/24(\varepsilon_3 + \varepsilon_2)$.

Γ_{sub} is compared to Γ_{free} for varying ε_3's in Fig. 2. Interestingly, in contrast to the ε_2 dependence of Γ_{free}, real-valued $\varepsilon_3 > 1$ universally suppresses decay [Fig. 2(a)] since $\mathbf{A}_I$ is opposite $\mathbf{A}$ within the particle, screening the coupling to electrons. Only when ε_3 is complex valued [Fig. 2(b)], indicating that the substrate has intrinsic losses, can energy transfer result in an increase above the free space LSP linewidth, pushing the LSP into a regime where Landau damping and near-field energy transfer become competitive. We stress, however, that this is due to intrinsic loss in the substrate not due to the enhancement of electron-hole pair generation, illustrating the difficulty in disentangling these processes.

Using Eq. (4) we can calculate the quantum-corrected substrate-dressed LSP energy as was done previously. This is plotted in Fig. 1(c) (the blue curve) with $\varepsilon_3 = 3$ for carbon, and we see that the modified resonance energies agree excellently with the EELS data [39] where the free space calculation fails. Since the previous calculation is simply a special case ($\varepsilon_3 = \varepsilon_2 = 1$) of Eq. (4), we have presented a single theory that quantitatively agrees with classical electrodynamics and all four experiments [36–39] over a wide range of particle sizes.

Our theory explicitly models LSP-electron interaction and dielectric environment effects but neglects intrinsic losses in bulk silver [45], ligand effects, and electron spill out while using a local dielectric function and a relatively simple approximation to the MNP electronic structure. This indicates that LSP-electron interaction dominates LSP loss at these sizes and that environmental effects play a much more significant role in determining quantum plasmon properties than previously thought [39].

Interestingly, in Fig. 1(c), the EELS data appear to shift off the substrate-modified calculation and to the free space calculation for $a \leqslant 3$ nm. Full-wave simulation of Maxwell's equations [46] explains this effect, showing that substrate-induced reductions in LSP energy are large for $a > 3$ nm but vanish for smaller particles. That this feature of the data can be qualitatively reproduced in simulations indicates that it is due to retardation and not a quantum effect.

We now extend the theory to incorporate an optical emitter, such as a quantum dot, fluorophore, substrate resonance, or second MNP to illustrate how LSP decay to electron-hole pairs is altered in more complex environments. As depicted in the inset of Fig. 3, we neglect the emitter's electronic structure and model it as a point dipole oscillating at frequency ω_{em} located a distance s from the MNP surface. Equation (1) now becomes

$$H_{\text{LSP-em}} = H_{\text{free}} + \left(\frac{V_{\text{em}}}{2}p_{\text{em}}^2 + \frac{\omega_{\text{em}}^2}{2V_{\text{em}}}q_{\text{em}}^2\right) - \mathbf{d}_{10}\cdot\mathbf{E}_{\text{em}}$$
$$- \frac{e}{2m_e c}\sum_i [\mathbf{p}_i \cdot \mathbf{A}_{\text{em}}(\mathbf{x}_i) + \mathbf{A}_{\text{em}}(\mathbf{x}_i)\cdot\mathbf{p}_i], \quad (5)$$

where p_{em} and q_{em} are the generalized emitter momentum and coordinate and $\mathbf{E}_{\text{em}}$ and $\mathbf{A}_{\text{em}}$ are the emitter electric field and vector potential. The mode volume V_{em} is defined in connection to the emitter dipole moment, which is assumed to be $\mathbf{d}_{\text{em}} = CV_{\text{em}}p_{\text{em}}\hat{\mathbf{z}}$, where C is a dimensionless constant that gives the results below general applicability. This Hamiltonian shows that, like the substrate, the emitter couples both to the LSP directly and to the individual electrons through $\mathbf{A}_{\text{em}}$.

The direct LSP coupling can again be diagonalized through transformation. This results in two hybridized LSP-emitter normal modes with eigenfrequencies defined by

$$\omega_{\pm}^2 = \omega_{\text{em}/10}^2\cos^2\theta + \omega_{10/\text{em}}^2\sin^2\theta$$
$$\pm\frac{2g\omega_{10}\omega_{\text{em}}}{\sqrt{V_{10}V_{\text{em}}}}\sin\theta\cos\theta, \quad (6)$$

and mode volumes,

$$V_{\pm} = V_{\text{em}/10}\frac{\omega_{\text{em}/10}^2}{\omega_{10/\text{em}}^2}\cos^2\theta + V_{\text{em}/10}\sin^2\theta$$
$$\pm\frac{2g\omega_{\text{em}/10}}{\omega_{10/\text{em}}}\sqrt{\frac{V_{\text{em}/10}}{V_{10/\text{em}}}}\sin\theta\cos\theta. \quad (7)$$

Here $\tan(2\theta) = 2g\omega_{10}\omega_{\text{em}}/\sqrt{V_{10}V_{\text{em}}}(\omega_{\text{em}}^2 - \omega_{10}^2)$, and $g = 2CV_{10}V_{\text{em}}(\varepsilon_1 - \varepsilon_2)/\sqrt{12\pi}(a+s)^3$.

The rotation angle θ characterizes the degree of mixing between the LSP and the emitter and is positive when $\omega_{\text{em}} > \omega_{10}$. In that case, the $-$ and $+$ modes correspond to the well-known in-phase and out-of-phase eigenmodes of a coupled dipole system [43,50]. At $\theta = 0^\circ$, when ω_{10} and ω_{em} are sufficiently detuned or the separation distance s is much larger than a, the LSP and emitter are essentially uncoupled, and the $-$ mode reduces to the LSP, whereas the $+$ mode reduces to the emitter. On the other hand, if ω_{10} and ω_{em} are degenerate or s is very small, θ approaches 45°, and the LSP and emitter are significantly mixed.

This transformation modifies the second coupling term in Eq. (5), and both the in-phase ($-$) and the out-of-phase ($+$) modes interact with electrons differently. Calculating these interaction terms, a perturbation theory can be carried out for each mode, again using $\mathbf{A}_{\text{em}}(\mathbf{x}_i) \approx \mathbf{A}_{\text{em}}(\langle \mathbf{x}_i \rangle)$. The resulting decay rates are

$$\Gamma_-(\omega_-, V_-) = \left|\frac{\omega_{\text{em}}}{\omega_{10}}\cos\theta - \sqrt{\frac{16\pi V_{\text{em}}}{3V_{10}}}\frac{Ca^3}{(a+s)^3}\sin\theta\right|^2$$
$$\times\,\Gamma_{\text{free}}(\omega_-, V_-),$$
$$\Gamma_+(\omega_+, V_+) = \left|\sqrt{\frac{V_{10}}{V_{\text{em}}}}\sin\theta + \sqrt{\frac{16\pi}{3}}\frac{\omega_{10}}{\omega_{\text{em}}}\frac{Ca^3}{(a+s)^3}\cos\theta\right|^2$$
$$\times\,\Gamma_{\text{free}}(\omega_+, V_+). \quad (8)$$

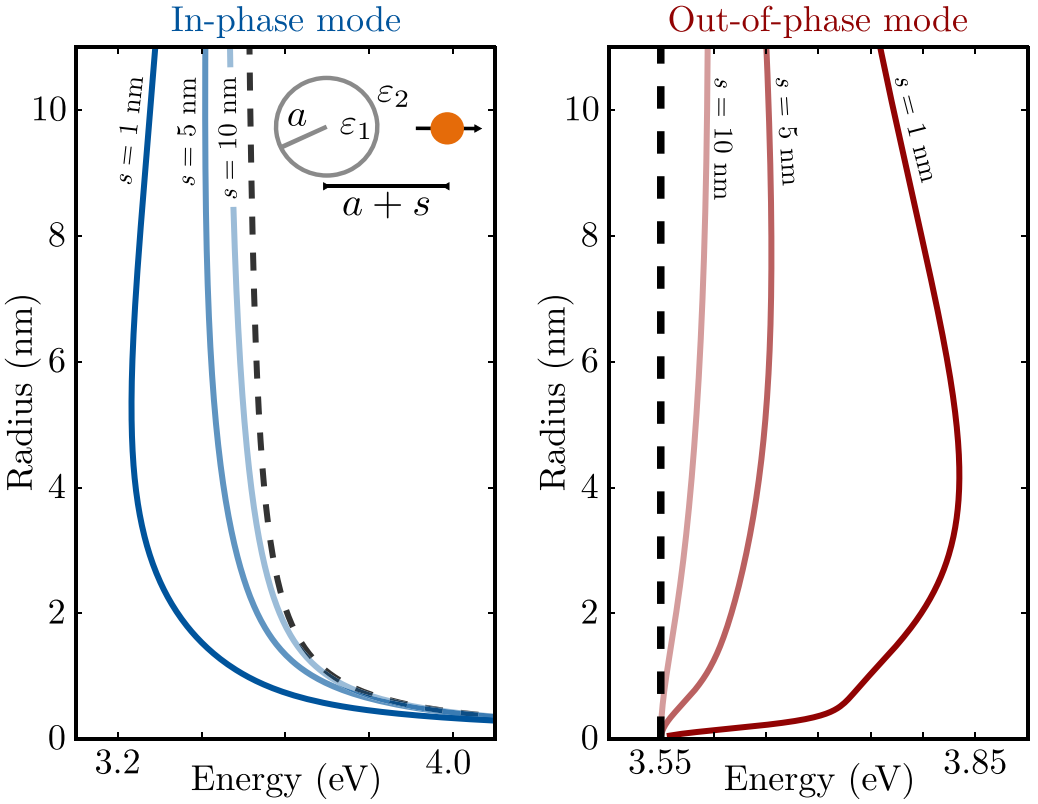

FIG. 3. Evolution of the renormalized in-phase (left) and out-of-phase (right) normal modes of the coupled MNP-optical emitter system (the inset) as a function of a for three separation distances $s = 1$, 5, and 10 nm. The in-phase mode tracks the uncoupled LSP (left, the black dashed line) and shifts to lower energies as the s decreases. Alternatively, the out-of-phase mode tracks the uncoupled emitter (right, the black dashed line) and shifts to higher energies as s decreases. Furthermore, as the MNP radius decreases, shifting of $\hbar\omega_{10}$ causes a rapid decoupling of the LSP and emitter, resulting in a rapid redshift of $\hbar\omega_{+}^{*}$.

Note that the emitter vector potential destructively interferes with the decay in the in-phase configuration where $\mathbf{A}$ and $\mathbf{A}_{\text{em}}$ are misaligned within the particle but constructively interferes in the out-of-phase configuration where $\mathbf{A}$ and $\mathbf{A}_{\text{em}}$ are aligned within the particle. This implies that, if the modes are mixed, the out-of-phase mode more efficiently decays to electronic excitations than the in-phase mode. This is in stark juxtaposition to the hybridized modes' coupling to near-field energy transfer and far-field radiation where the in-phase mode's larger dipole moment makes it the more efficiently decaying hybrid resonance [43].

Equation (8) can be used just as the decay rates previously to calculate the quantum-corrected eigenenergies $\hbar\omega_{\pm}^{*}$. For the case where the emitter is another silver nanosphere with fixed radius (4 nm, $\hbar\omega_{\text{em}} = 3.55$ eV), we plot in Fig. 3 the eigenenergies as a function of a for three separation distances $s = 1$, 5, and 10 nm, and we compare to the uncoupled ($g = 0$) energies (the black dashed curves). We see that $\hbar\omega_{-}^{*}$ qualitatively tracks the LSP and shifts to lower energies as s decreases with a maximal shift when $\omega_{10} \sim \omega_{\text{em}}$. On the other hand, $\hbar\omega_{+}^{*}$ tracks $\hbar\omega_{\text{em}}$ and shifts to higher energies as s decreases.

Interestingly, as a decreases, the shift of the in-phase mode becomes severe enough that the LSP and emitter effectively decouple and the out-of-phase mode rapidly collapses back to the uncoupled emitter energy, giving it a dramatically different a dependence. This pronounced change highlights previously unexplored quantum effects on plasmon hybridization. Measurement of the hyrbridized LSP-emitter modes' dependence on MNP size would support the prediction that the out-of-phase mode more effectively couples to electrons, suggesting new strategies to disentangle LSP decay pathways.

In this Rapid Communication we have developed an analytic theory of noble-metal LSPs in optically active environments. By incorporating dielectric environment effects on LSP-electron interaction, our theory agrees with Mie theory [48], photofragmentation spectroscopy [36], matrix deposition spectroscopies [37,38], and EELS [39] over orders-of-magnitude changes in size with only two parameters defined by bulk dielectric data [45], indicating that environmental effects play a significant role in plasmonic Landau damping.

Current work on optimizing plasmonic systems for charge manipulation often relies on indirect spectral signals to elucidate nanoscale behavior. Experiments are in turn required to design systems which isolate Landau damping from other decay pathways, such as near-field energy transfer and far-field radiation. Our approach disentangles LSP-electron and LSP-photon interactions by showing that the out-of-phase mode of a hybrid LSP-emitter system more strongly couples to electrons whereas the in-phase mode more strongly couples to photons. As a whole, this Rapid Communication shows that just as LSP radiative properties are strongly environmentally dependent, LSP decay to electron-hole pairs can be suppressed or enhanced by environmental

factors. Our approach therefore provides an analytic platform to tailor the optoelectronic properties of open plasmonic systems.

We thank D. Rim for useful discussions regarding the mathematics, S. C. Quillin for assistance with the numerical simulations, and Professor H. Petek for critically reading and editing the Rapid Communication. This Rapid Communication was partially supported by the NSF under Awards No. DGE-1256082 (N.T.) and No. CHE-1664684 (D.J.M.), as well as by the DOE Basic Energy Sciences under Award No. DE-SC0018040 (D.J.M.).

[1] W. L. Barnes, A. Dereux, and T. W. Ebbesen, Nature (London) **424**, 824 (2003).
[2] R. F. Oulton, V. J. Sorger, D. Genov, D. Pile, and X. Zhang, Nat. Photonics **2**, 496 (2008).
[3] G. Baffou and R. Quidant, Laser Photonics Rev. **7**, 171 (2013).
[4] G. Baffou, R. Quidant, and F. J. García de Abajo, ACS Nano **4**, 709 (2010).
[5] M. L. Brongersma, N. J. Halas, and P. Nordlander, Nat. Nanotechnol. **10**, 25 (2015).
[6] S. F. Tan, L. Wu, J. K. Yang, P. Bai, M. Bosman, and C. A. Nijhuis, Science **343**, 1496 (2014).
[7] S. Linic, P. Christopher, and D. B. Ingram, Nature Mater. **10**, 911 (2011).
[8] W. Du, T. Wang, H.-S. Chu, L. Wu, R. Liu, S. Sun, W. K. Phua, L. Wang, N. Tomczak, and C. A. Nijhuis, Nat. Photonics **10**, 274 (2016).
[9] L. D. Landau, Zh. Eksp. Teor. Fiz. **16**, 574 (1946).
[10] K. Wu, J. Chen, J. McBride, and T. Lian, Science **349**, 632 (2015).
[11] V. Schweikhard, A. Grubisic, T. A. Baker, I. Thomann, and D. J. Nesbitt, ACS Nano **5**, 3724 (2011).
[12] A. Hoggard, L.-Y. Wang, L. Ma, Y. Fang, G. You, J. Olson, Z. Liu, W.-S. Chang, P. M. Ajayan, and S. Link, ACS Nano **7**, 11209 (2013).
[13] G. Li, C. Cherqui, N. W. Bigelow, G. Duscher, P. J. Straney, J. E. Millstone, D. J. Masiello, and J. P. Camden, Nano Lett. **15**, 3465 (2015).
[14] E. M. Purcell, Phys. Rev. **69**, 681 (1946).
[15] R. R. Chance, A. Prock, and R. Silbey, Adv. Chem. Phys. **37**, 65 (1978).
[16] A. Kawabata and R. Kubo, J. Phys. Soc. Jpn. **21**, 1765 (1966).
[17] W. A. Kraus and G. C. Schatz, J. Chem. Phys. **79**, 6130 (1983).
[18] U. Kreibig and L. Genzel, Surf. Sci. **156**, 678 (1985).
[19] C. Yannouleas and R. A. Broglia, Ann. Phys. (N.Y.) **217**, 105 (1992).
[20] G. Weick, R. A. Molina, D. Weinmann, and R. A. Jalabert, Phys. Rev. B **72**, 115410 (2005).
[21] R. C. Monreal, T. J. Antosiewicz, and S. P. Apell, New J. Phys. **15**, 083044 (2013).
[22] G. Toscano, J. Straubel, A. Kwiatkowski, C. Rockstuhl, F. Evers, H. Xu, N. A. Mortensen, and M. Wubs, Nat. Commun. **6**, 7132 (2015).
[23] A. Brandstetter-Kunc, G. Weick, D. Weinmann, and R. A. Jalabert, Phys. Rev. B **91**, 035431 (2015).
[24] P. Echenique, J. Pitarke, E. Chulkov, and A. Rubio, Chem. Phys. **251**, 1 (2000).
[25] A. García-Lekue, J. M. Pitarke, E. V. Chulkov, A. Liebsch, and P. M. Echenique, Phys. Rev. B **68**, 045103 (2003).
[26] R. Sundararaman, P. Narang, A. S. Jermyn, W. A. Goddard III, and H. A. Atwater, Nat. Commun. **5**, 5788 (2014).
[27] M. Bernardi, J. Mustafa, J. B. Neaton, and S. G. Louie, Nat. Commun. **6**, 7044 (2015).
[28] H. Haberland, Nature (London) **494**, E1 (2013).
[29] X. Chen, J. E. Moore, M. Zekarias, and L. Jensen, Nat. Commun. **6**, 8921 (2015).
[30] J. Lermé, J. Phys. Chem. C **115**, 14098 (2011).
[31] K.-Y. Lian, P. Sałek, M. Jin, and D. Ding, J. Chem. Phys. **130**, 174701 (2009).
[32] C. M. Aikens, S. Li, and G. C. Schatz, J. Phys. Chem. C **112**, 11272 (2008).
[33] V. Bonačić-Koutecky, V. Veyret, and R. Mitrić, J. Chem. Phys. **115**, 10450 (2001).
[34] K. Yabana and G. F. Bertsch, Phys. Rev. A **60**, 3809 (1999).
[35] U. Kreibig and M. Vollmer, *Optical Properties of Metal Clusters* (Springer, Berlin, Heidelberg, 2013), Vol. 25 .
[36] J. Tiggesbäumker, L. Köller, K.-H. Meiwes-Broer, and A. Liebsch, Phys. Rev. A **48**, R1749 (1993).
[37] K.-P. Charlé, L. König, S. Nepijko, I. Rabin, and W. Schulze, Cryst. Res. Technol. **33**, 1085 (1998).
[38] W. Harbich, S. Fedrigo, and J. Buttet, Z. Phys. D **26**, 138 (1993).
[39] J. A. Scholl, A. L. Koh, and J. A. Dionne, Nature (London) **483**, 421 (2012).
[40] L. Zhou, Y. Tan, J. Wang, W. Xu, Y. Yuan, W. Cai, S. Zhu, and J. Zhu, Nat. Photonics **10**, 393 (2016).
[41] A. G. Curto, G. Volpe, T. H. Taminiau, M. P. Kreuzer, R. Quidant, and N. F. van Hulst, Science **329**, 930 (2010).
[42] C. L. Haynes, A. D. McFarland, and R. P. Van Duyne, Anal. Chem. **77**, 338 (2005).
[43] N. Thakkar, C. Cherqui, and D. J. Masiello, ACS Photonics **2**, 157 (2015).
[44] S. Lecoultre, A. Rydlo, and C. Félix, J. Chem. Phys. **126**, 204507 (2007).
[45] P. B. Johnson and R. W. Christy, Phys. Rev. B **6**, 4370 (1972).
[46] See Supplemental Material at http://link.aps.org/supplemental/10.1103/PhysRevB.97.121403 for a complete derivation of all the presented results.
[47] C. Cherqui, N. Thakkar, G. Li, J. P. Camden, and D. J. Masiello, Annu. Rev. Phys. Chem. **67**, 331 (2016).
[48] G. Mie, Ann. Phys. **330**, 377 (1908).
[49] K. Cahill, Phys. Rev. E **85**, 051921 (2012).
[50] E. Prodan, C. Radloff, N. J. Halas, and P. Nordlander, Science **302**, 419 (2003).